Dual-Mass Flywheel with Torque Limiter: An Effective Solution for Overtorque Suppression in Automotive Transmission

Dual-mass flywheel with torque limiter: an effective solution for overtorque suppression in automotive transmission

Enrico Galvagno, Alessandro Vigliani, and Giuseppe Calenda

DIMEAS, Politecnico di Torino

Citation: Galvagno, E., Vigliani, A. and Calenda, G., "Dual-Mass Flywheel with Torque Limiter: An Effective Solution for Overtorque Suppression in Automotive Transmission," SAE Technical Paper 2020-01-1016, 2020, doi:10.4271/2020-01-1016.

Abstract

During some critical maneuvers, transmission systems using Dual Mass Flywheel (DMF) may experience overtorques, which could lead to structural damages of the transmission components. In a dual mass flywheel, total inertia is divided into two parts: a primary mass connected to the engine and a secondary mass to the transmission. The torque delivered by the engine is transferred from one mass to the other through a drive plate and a set of arc springs, the latter absorbing the torsional oscillations coming from internal combustion engine and the shocks caused by fast clutch engagements. This paper investigates overtorque issues and proposes a solution based on a torque limiter, consisting of a friction clutch inserted between the two masses, that limits the maximum torque transmitted through it. The basic idea is to replace the classic flat drive plate with a tapered drive plate that functions as a Belleville spring. The experimental analysis carried out on dedicated benches has tested the elastic characteristic of the tapered drive plate, the durability of friction pads and the variation of the slipping torque over time. This article analyzes the torque limiter benefits through a detailed torsional dynamic model implemented in Simcenter Amesim. Overtorque phenomena are excited during cranking-in-gear vehicle launch tests on different slopes. Furthermore, a simplified multi-degree of freedom transmission model developed in Matlab/Simulink is shown; it allows calculating frequency response functions, natural frequencies, mode shapes and overtorque limitation. The comparison between the two models revealed that even the simplified model is capable of predicting the main dynamic aspects involved in the overtorque phenomenon and the positive effect of the torque limiter.

Introduction

Dual Mass Flywheel is a component used to reduce vehicle driveline noise and vibrations in high fluctuating torque applications, e.g. diesel engine and some hybrid electric powertrains. These vibrations reduce driver comfort and could damage driveline components in the long term. Beside passive solution, like the one presented in the paper, the coordinated control of powertrain and active brake system are alternative effective solutions to mitigate driveline vibrations [1,2].

In a conventional powertrain with a small displacement gasoline engine, next to engine flywheel there is typically a clutch disc with torsional damper: this configuration is known as Single Mass Flywheel (SMF). In more demanding applications, this solution is no more satisfactory and so it is substituted by the Dual Mass Flywheel. The solution adopted in a Dual Mass Flywheel is to use two flywheels, instead of a unique solid disk, linked by long-stroke arc springs with low torsional stiffness and friction dampers. A drive plate mounted on the secondary flywheel receives torque from the springs and delivers it downstream to the transmission system.

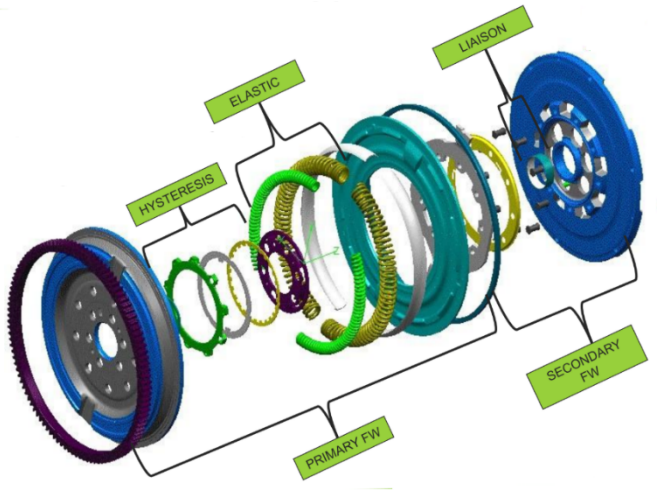

Figure 1. DMF exploded view

Figure 1 shows an exploded view of a DMF: the primary flywheel is bolted to the engine and has a ring gear for the engagement with the starter. The DMF springs ensure the elastic energy storage for the torsional oscillations; furthermore, the lower stiffness, if compared with a SMF solution, allows to shift resonance below the idle engine speed [3] and so outside the most frequent working range of the engine. The elastic and inertial elements continuously exchange energy during vibration while the hysteresis devices dissipate part of this energy thus allowing to reduce the vibration amplitude especially when crossing the torsional damper resonance.

Transmission torsional dynamics can be investigated through lumped parameter models, possibly validated with experimental data as presented in [4]. By means of these models, it is possible to obtain typical frequency response functions like those shown in Figures 2-4. Figure 2 shows the effect of variations of the torsional damper spring stiffness k on its resonance frequency, i.e. the second peak in the frequency response function (see Figures 2-4).

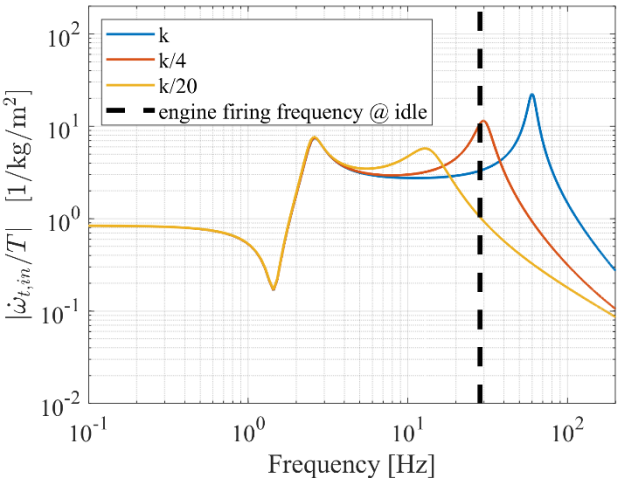

Figure 2. effect of torsional damper stiffness on frequency response (primary shaft acceleration over engine torque irregularity)

The role of the mass moment of inertia distribution I_1/I_2, I_1 on the engine side and I_2 on the gearbox side, is analyzed in Figure 3: the lower this ratio, the more the second peak is shifted towards lower frequencies. The curves shown in Figure 3 are obtained with a constant total DMF inertia $I_1 + I_2$. Obviously, a small value of the secondary inertia will lead the system to work similarly to the SMF configuration. Hence, DMF ensures better filtering than SMF, since lower stiffness combined with a different inertia distribution shift the torsional damper resonance below the engine idle speed, thus reducing the amount of torsional vibration transferred to the gearbox input shaft, except during engine start and stop transients.

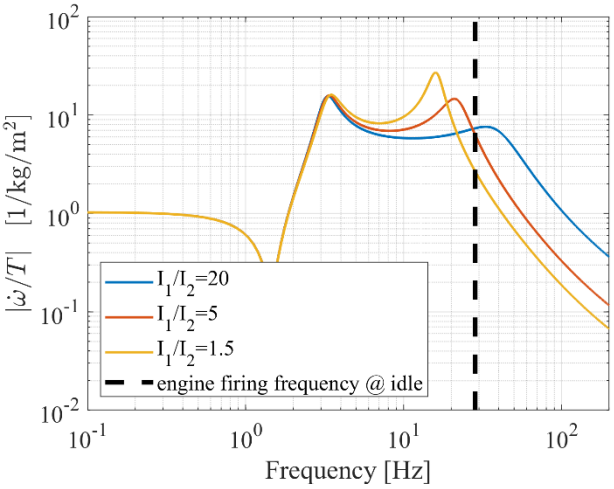

Figure 3. effect of inertia distribution on frequency response (primary shaft acceleration over engine torque irregularity)

The effect of DMF viscous damping is shown in Figure 4: close to the torsional damper resonance, damping reduces the vibration amplitude; conversely, in the normal working range of the engine, i.e., above the engine firing frequency at idle, transmissibility increases with damping.

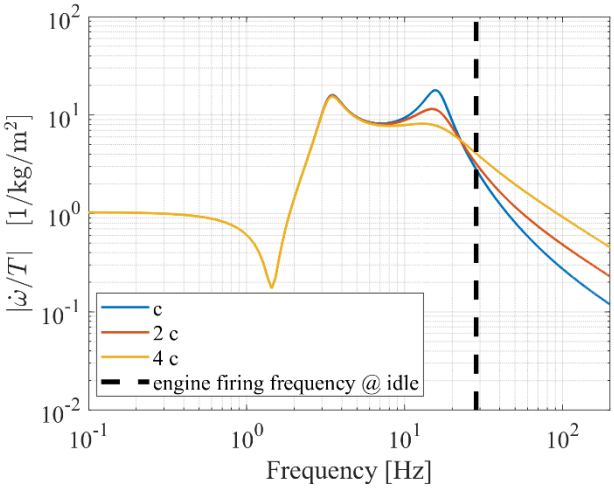

Figure 4. DMF response function for different damping coefficients

Particular attention must be paid in evaluating the engine start-up phase with a DMF, due to resonance crossing: a sensitivity analysis (in terms of DMF inertia, stiffness and damping) is necessary to minimize driveline oscillations [5]. The torsional dynamic behavior of a DMF is investigated both numerically and experimentally in [6], where a lumped parameter model of a torsional test rig considering two different models for the DMF damping (viscous and hysteretic) is proposed.

In addition to classic DMF, many advanced solutions have been designed, for example the Long Travel Damper DMF that has a particular drive plate typically with six sets of springs integrated. The classic arc springs and the new ones work in parallel. This solution is particularly useful at high engine speed where the centrifugal force on arc springs increases the hysteretic effect (poor vibrations filtering) [7]. Another solution is the Centrifugal Pendulum-type absorber DMF: in this case there are additional masses vibrating in opposition to the torsional vibration of the engine. The pendulum is tuned on the firing engine order, thus helping to overcome DMF limits whose isolation characteristic is fixed in frequency, while the excitation is related to engine orders, hence proportional to the engine speed. By reducing the engine speed, the filtering effect of classical DMF becomes increasingly smaller [8], while the pendulum type is able to track the order thus giving high isolation performance in the whole engine speed range.

The goal of this study is to analyze overtorques, to propose a technical solution and then to verify its efficacy in simulation. In [9] some causes that can generate overtorques such as a rapid clutch engagement with a high speed difference between engine and primary shaft, or torsional impacts due to DMF resonance crossing, are shown.

This paper illustrates, through the dynamic analysis of the mechanical system, the main advantage that a torque limiter integrated in a DMF provides to avoid overtorques. The basic idea is to substitute the classic flat drive plate with a tapered drive plate that works as a Belleville spring (Figure 5). The tapered drive plate is placed between two retainer plates (Figure 6), which are riveted one to the other. The

retainer plates impose a deformation to the Bellville spring and so the desired axial preload required by the application is generated.

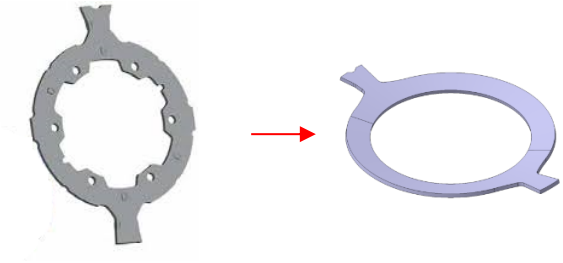

Figure 5. Drive plate design change for torque limiter construction: from flat (left) to tapered (right).

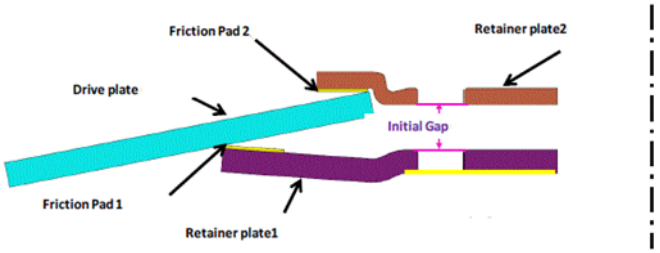

Figure 6. Cross-section of the torque limiter before applying the axial load.

As shown in Figure 6, friction pads are built-in on the inner surface of the retainer plates, facing to the drive plate. The torque limiter slip is triggered when the torque passing through the drive plate exceeds the designed slipping torque, depending on geometry, Belleville's axial load and friction coefficient.

In the first part of the paper, the authors describe the torque limiter design and working principle. After that, the experimental testing procedure to measure force-deflection curve of the tapered drive plate is presented and the results compared with analytical curves. Torsional tests on a dedicated test bench are shown to verify that torque limiter works in the proper way for the required number of cycles.
In the following part, a detailed torsional model implemented in Amesim is shown, to simulate abuse tests with overtorque peaks. Hence, the dynamic benefits introduced by a torque limiter are clearly highlighted. Furthermore, a modal analysis is carried out to estimate the natural frequency of the torsional damper and to easily identify resonance crossing in the simulation results.
The last part proposes a simplified transmission model in Matlab-Simulink. Natural frequencies, mode shapes and frequency response functions of the dynamic system with the torque limiter in adherence are calculated. The same abuse test causing overtorque peaks investigated with the detailed Amesim model is simulated with the simplified model, which is adequate to catch the main dynamic effects of the torque limiter on transmission shock and vibration.

Torque Limiter design

With reference to Figure 7, the torque limiter is composed of:

- a tapered drive plate acting as a Belleville spring;
- two retainer plates that slip, with respect to the drive plate, when the slipping torque is reached;
- two friction surfaces where the dissipation required to cut torque peaks takes place.

The drive plate in the assembled configuration is in flat position thanks to retainers riveting, thus generating the required spring preload. The slipping torque is proportional to Belleville axial force (in flat position), friction coefficient (between friction pads and drive plate) and radial position of friction surfaces.

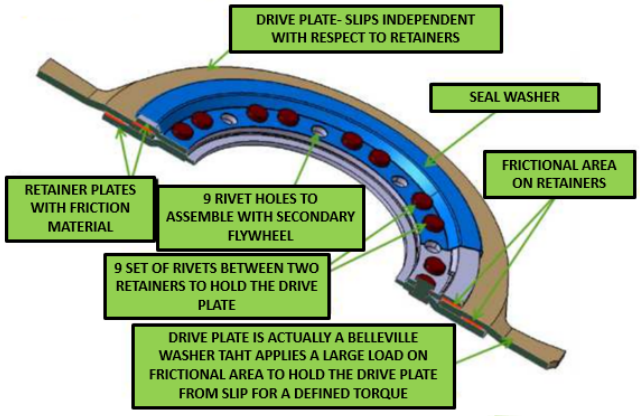

Figure 7. Torque limiter design

During compression, the reaction force in the axial direction increases following Belleville nonlinear spring characteristic; this characteristic has been experimentally determined thanks to tests on a dedicated bench equipped with a manual press and a force-displacement measuring system.

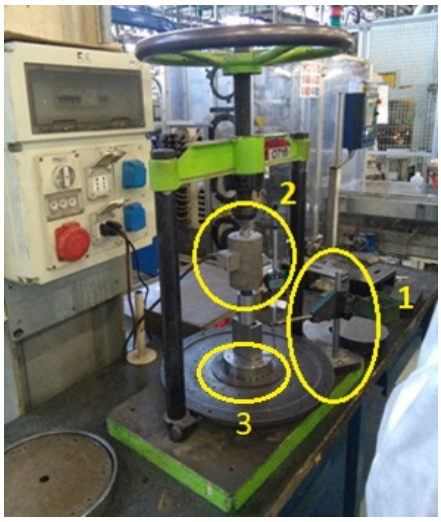

Figure 8. Press bench for drive plate axial compliance characterization.

The experimental apparatus, shown in Figure 8, is composed by a manual press, a comparator (1) that measures the linear displacement during compression and a load cell (2) to measure reaction force of test component (3). The Belleville spring characteristic depends on the

height to thickness ratio (h/t) as shown in Figure 9, and it is highly nonlinear (Figure 10).

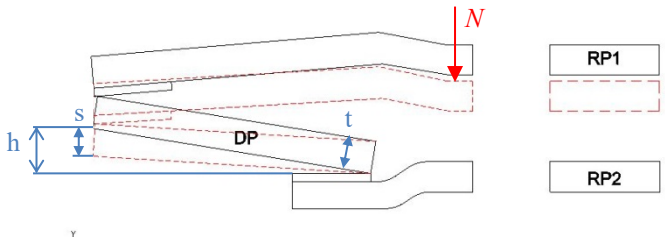

Figure 9. Drive plate deflection: in solid line the unladen configuration and in dashed lines a generic loaded configuration with axial load N and spring deformation s.

Figure 9 shows the geometrical parameters s, t and h determining the elastic behavior of the spring. Two configurations are depicted, the initial one, when no load is applied to the spring, solid lines, and a generic configuration characterized by a spring displacement s and a normal load N, dashed lines.

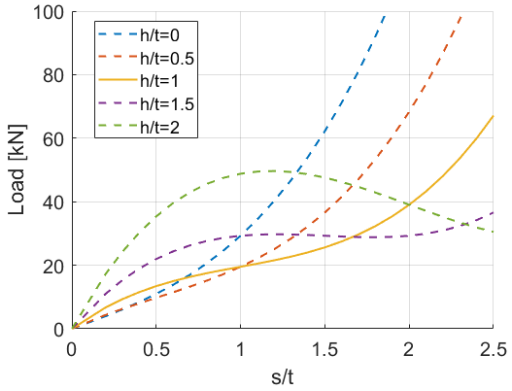

Figure 10. Spring characteristic for different h/t values

The choice of h/t in the range 1÷1.5, ensures a digressive characteristic with an almost horizontal slope in the neighborhood of the installation length of the spring, i.e. $s/t = h/t$ for a flattened spring (deflection equal to the unladen spring height: $s = h$).
This is a positive aspect for two main reasons:

- low local spring stiffness in the neighborhood of the nominal working point is suitable to minimize variability of the axial force due to unavoidable friction material wear;
- the spring should be as flat as possible in the assembled configuration to guarantee a uniform distribution of contact pressures all over the friction pads surface.

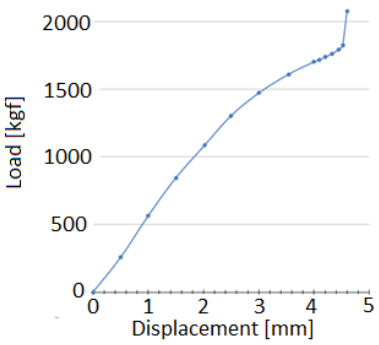

Figure 11. Experimental drive plate elastic characteristic with $h/t = 1$.

Figure 11 illustrates the measured elastic characteristic of the drive plate. The final slope increase (last point) is due to an incorrect constraint of the drive plate on the test bench, which does not allow the spring to overturn and thus it is not representative of the ideal behavior of the spring, as reported in Figure 10.

The following equation allows calculating the spring reaction force N as a function of deflection s according to the DIN standard [10]:

$$N = \frac{4E}{1-\mu^2}\,\frac{t^4}{K_1 D_e^2}\,\frac{s}{t}\left[\left(\frac{h}{t}-\frac{s}{t}\right)\left(\frac{h}{t}-\frac{s}{2t}\right)+1\right] \quad (1)$$

$$K_1 = \frac{\frac{1}{\pi}\left(\frac{\delta-1}{\delta}\right)^2}{\frac{\delta+1}{\delta-1}-\frac{2}{\ln\delta}} \quad (2)$$

$$\delta = \frac{D_e}{D_i} \quad (3)$$

where:

- E: elastic modulus
- μ: Poisson's ratio
- t: thickness
- D_e: external diameter (= 2 R_{ext} in Figure 12)
- D_i: internal diameter (= 2 R_{int} in Figure 12)
- h: free height

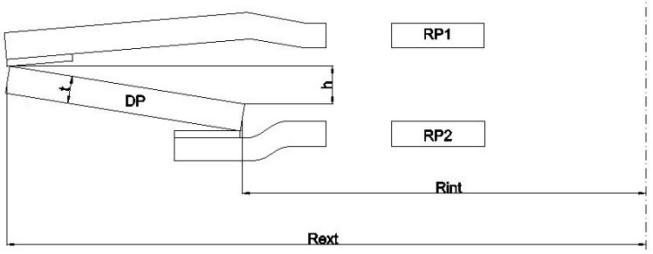

Figure 12. Torque limiter design parameters

By comparing the solid line in Figure 10, i.e. the theoretical curve with $h/t = 1$, with Figure 11, good agreement with experimental characteristic can be observed.

One of the most critical aspects for torque limiter design is the selection of proper friction material for the pads; this choice impacts

significantly on torque limiter reliability and must be carefully verified through specific tests on a torsional test bench. To this aim, the torque limiter has been screwed from one side to a flywheel, connected to the electric motor of the bench, while the other side is fixed to the bench structure by its fingers. Tests consist in imposing a relative motion between retainers and drive plate; in particular a sinusoidal angular displacement (at a frequency of 0.4 Hz) has been applied by the motor to simulate the load cycles. The friction material must ensure the required slipping torque for a predefined number of cycles. Figure 13 shows the torque vs angular displacement curve experimentally evaluated during the application of the first 50 cycles. It can be observed that slipping torque is fairly constant in these cycles.

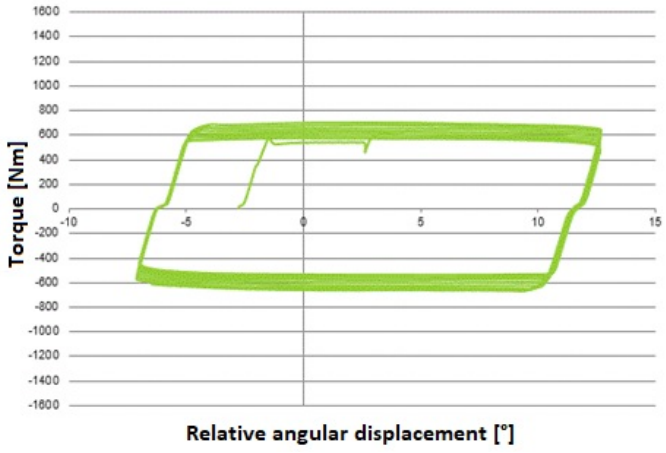

Figure 13. Torque limiter load cycle

Critical maneuver generating overtorques

A start-up maneuver with the manual transmission in first gear and the main clutch closed, called Cranking In Gear (CIG), is considered. During CIG start, the vehicle inertia applies an additional load through the driveline, thus requiring the starter motor to do more work, resulting in longer start-up times. Hence, there will be a longer dwell time in DMF resonance, resulting in DMF torsional impacts. Maneuvers like CIG in forward up-hill or while passing an obstacle (e.g. rocks or big stones) represent the most critical conditions for DMF impacts. As a result, instantaneous torque increases up to critical values if a torque limiter is not used.
In [11] there is an effective analysis of the typical starting phase with the main clutch disengaged, in particular it is explained how to overcome engine stalling in resonance by acting on the starter electric motor torque map, also considering different amount of torque irregularities from the internal combustion engine. Thus, a poor starting behavior in which there is not enough energy for revving up can be avoided.
In this paper an abuse test is analyzed, i.e. the starting phase with the first gear engaged and the clutch closed; different road slopes are examined.

Detailed Amesim model

The detailed powertrain model (Figure 14) implemented in Amesim is composed of the following subsystems:

- engine;
- DMF with torque limiter;
- damped disc;
- gearbox;
- driveline for rear wheel drive, composed of a front propeller shaft and a rear propeller shaft linked by a coupling, and an open differential that splits the torque on the two half shafts.

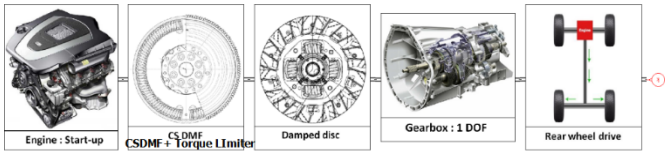

Figure 14. Amesim vehicle model scheme

Table 1 contains the numerical values of the inertial and elastic parameters of the detailed transmission model.

I_{ENGINE}	0.0420 kg $\cdot m^2$
$I_{PRIMARY\ FLYWHEEL}$	0.13 kg $\cdot m^2$
$I_{SECONDARY\ FLYWHEEL}$	0.095 kg $\cdot m^2$
I_{CLUTCH}	0.0110 kg $\cdot m^2$
$I_{PRESSURE\ PLATE}$	0.110 kg $\cdot m^2$
$I_{DRIVE\ PLATE}$	0.0040 kg $\cdot m^2$
$I_{PROP,FRONT}$	0.0130 kg $\cdot m^2$
$I_{PROP,REAR}$	0.0115 kg $\cdot m^2$
$I_{HALFSHAFT}$	0.0135 kg $\cdot m^2$
k_{DMF}	Piecewise linear: 5 Nm/° and 14 Nm/°
$k_{PROP,FRONT}$	550 $Nm/°$
$k_{PROP,REAR}$	660 $Nm/°$
$k_{HALFSHAFT}$	270 $Nm/°$

Table 1. Inertia and stiffness values

The input torque is the sum of engine torque and electric motor torque (starter). The engine torque as function of the crankshaft angle is used as input for the simulation, as reported in Figure 15. It is an estimate made starting from the measure of the instantaneous engine speed through a dedicated pick-up sensor. It includes:

- inertial forces due to reciprocating masses;
- intake, compression and expansion phases;
- pilot injections.

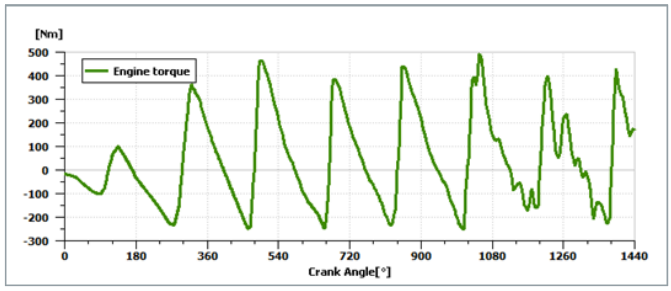

Figure 15. Engine experimentally estimated torque

The starter torque is computed as a function of its rotational speed from the steady-state electric motor torque map in Figure 16.

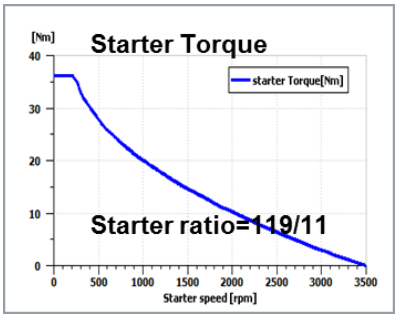

Figure 16. Starter torque map

The Dual Mass Flywheel has been modeled trough two inertia blocks simulating primary and secondary flywheels separated by multiple rotary inertias for arc springs (Figure 17).

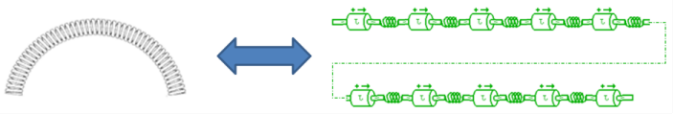

Figure 17. Arc springs modeling in Amesim (simplified for the sake of clarity).

In Figure 18, forces acting on each elementary mass, in which arc springs are discretized, are shown.

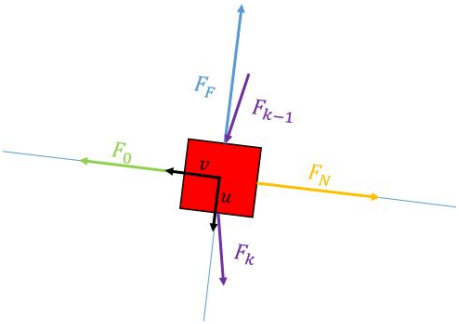

Figure 18. Forces applied on elementary mass

More specifically, the model takes into account:

- F_{k-1}: previous elementary spring force;
- F_k: next elementary spring force;
- F_F: friction force exchanged with the primary flywheel;
- F_0: preload force;
- F_N: total normal reaction force applied by the primary flywheel (includes the centrifugal force).

The torque limiter is a friction coupling between drive plate and secondary flywheel and has been modeled through a rotary Coulomb and stiction friction model (Figure 19).

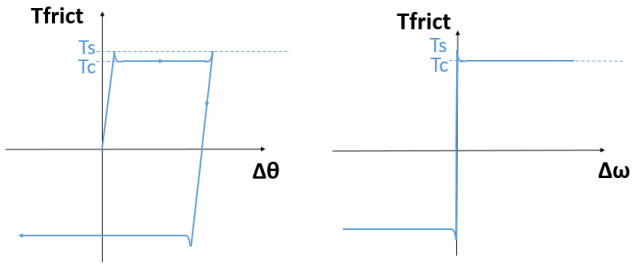

Figure 19. Friction torque as a function of relative displacement and speed

The selected friction model in Amesim takes into account the static and dynamic friction torque together with the stick stiffness and damping; the model equations are:

$$T_{friction} = \begin{cases} k\,\Delta\theta + c\,\Delta\omega & \text{if } |\Delta\theta| < \Delta\theta_{TH} \rightarrow \text{stick} \\ T_c\,\text{sgn}(\Delta\omega) & \text{if } |\Delta\theta| > \Delta\theta_{TH} \rightarrow \text{slip} \end{cases} \quad (4)$$

where

- k stick torsional stiffness
- c viscous friction during stiction
- T_c dynamic friction torque
- $\Delta\theta_{TH}$ stick displacement threshold

Torsional damper mode

A linearized version of the previous model was used to evaluate the natural frequencies and modal shapes of the system (Figure 20).

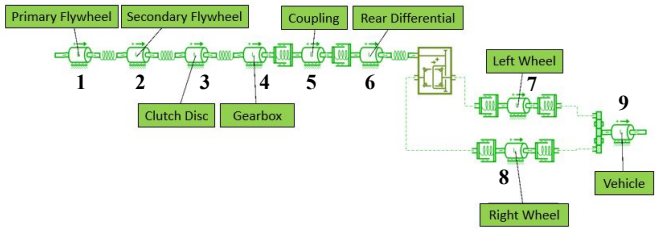

Figure 20. Vehicle simplified model in Amesim for modal analysis

The system has multiple resonance frequencies, in particular the torsional damper mode is at 9 Hz: Figure 21 shows the first two inertias 1 and 2 (representing primary and secondary flywheel) in phase opposition at this frequency.

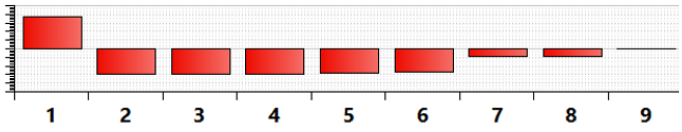

Figure 21. Torsional damper mode. The numbers correspond to the nine DOFs shown in Figure 20.

When dealing with internal combustion engines, the main excitation order is the one associated with cylinders firing. For instance, in a four-cylinder four-stroke engine there are four events of combustion for each thermodynamic cycle, so the 2nd order is the most important. The firing excitation frequency in this case is:

$$f_{firing}[\text{Hz}] = \frac{n[\text{rpm}]}{60} \cdot \frac{n_{cil}}{\frac{n_{strokes}}{2}} = \frac{n[\text{rpm}]}{30} \quad (5)$$

Considering the DMF resonance at 9 Hz, equation (5) gives a DMF critical speed of 270 rpm.

Simulation results of the detailed model

The aim of simulations is to analyze the DMF dynamic behavior during cranking in gear tests at different road slopes: changing the grade resistance causes the DMF to work at different rotational speeds. On flat road, Figure 22, the starter contributes to accelerate the vehicle up to idle speed without significant issues. It can be noted that the starter disengages when fuel injections start at around 300 rpm. In the first part of the chart, a resonance area is visible, where speed oscillation rises. The resonance zone is rapidly crossed so speed and torque do not increase up to critical values.

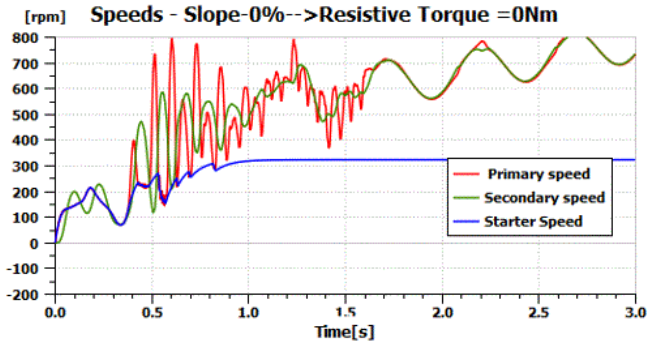

Figure 22. Speed without torque limiter at 0% slope

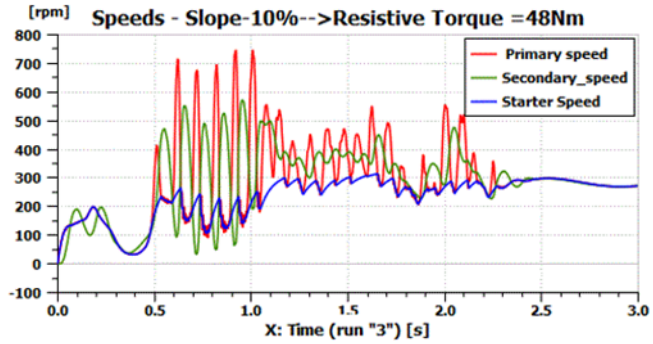

Figure 23. Speed without torque limiter at 10% slope

Increasing the road slope, and so the resistive torque, the starter is no more able to accelerate the vehicle up to engine idle speed so the DMF works at its torsional critical speed (around 270 rpm) for a longer time (Figure 23). Consequently, there are higher speed oscillations and dangerous overtorques are generated. By comparing the torque trends reported in Figure 24 and 25, when the slope increases and DMF works longer at resonance frequency, overtorque peaks appear. Torque limiter has the task of reducing these peaks by slipping. In Figure 26, thanks to torque limiter, torque on secondary flywheel saturates at 1240 Nm, so arc springs are not excessively stressed.

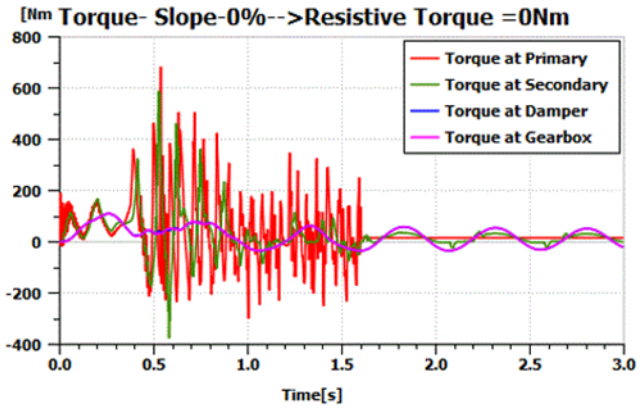

Figure 24. Torque without torque limiter at 0% slope

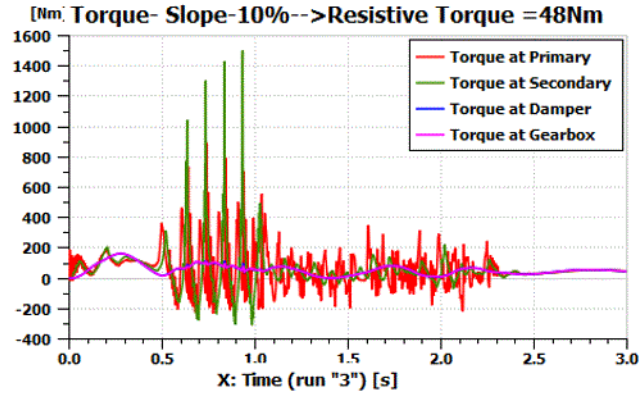

Figure 25. Torque without torque limiter at 10% slope

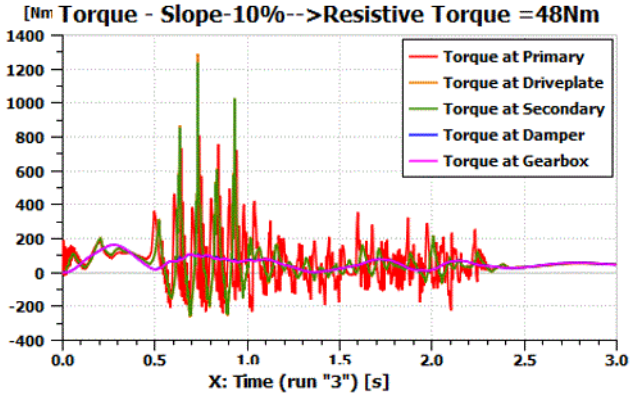

Figure 26. Torque with torque limiter at 10% slope

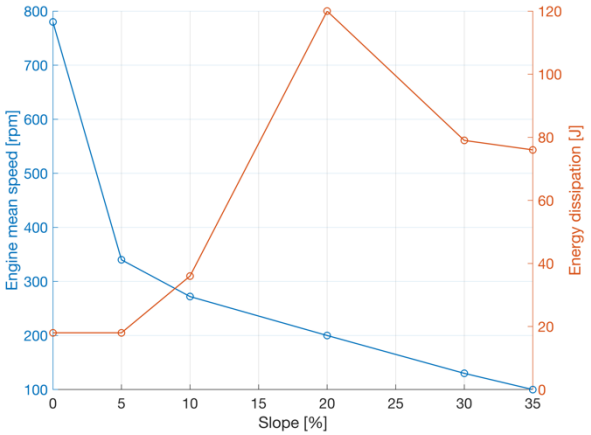

Figure 27. Energy dissipation graph

Figure 27 shows the effect of different road slope on engine mean speed and energy dissipated during the CIG test. With a slope of 20%, the energy dissipation operated by the torque limiter is maximum. On the left side of the graph, i.e. at low slopes, an increase in the slope causes higher overtorque peaks, since the powertrain oscillates harder during the climb and the DMF is more stressed. As a result, more and more energy is dissipated during the slip. After the maximum, the trend is reversed, and the energy dissipation starts to decrease because the starter is no longer able to accelerate the engine until it reaches the critical speed condition.

Simplified Matlab-Simulink model

This section introduces a simplified 3-4 dof dynamic model that can be used to investigate, at least qualitatively, the concept of overtorque suppression via torque limiter.

3 dof model

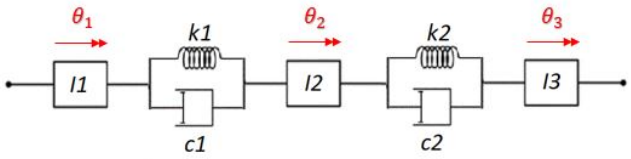

Figure 28. Three d.o.f. vehicle model

The 3 dof vehicle model is made up of three rotary inertias and two springs and dampers (Figure 28), where:

- I_1 is the engine and primary flywheel moment of inertia;
- I_2 is the sum of inertias of drive plate, secondary flywheel, clutch driven disc, pressure plate and front propeller shaft;
- I_3 is the sum of inertias of rear propeller shaft, half shafts, tires and vehicle;
- k_1 is the torsional damper stiffness;
- c_1 is the equivalent viscous damping coefficient due to the hysteresis elements in DMF;
- k_2 is propshaft and half shaft stiffness;
- c_2 is propshaft and half shaft damping;

These stiffnesses, moments of inertia and damping coefficients are equivalent quantities evaluated at the engine shaft. The equations of motion for the 3 dof model are:

$$I_1\ddot{\theta}_1 + k_1(\theta_1 - \theta_2) + c_1(\dot{\theta}_1 - \dot{\theta}_2) = 0 \quad (6)$$

$$I_2\ddot{\theta}_2 - k_1(\theta_1 - \theta_2) - c_1(\dot{\theta}_1 - \dot{\theta}_2) + k_2(\theta_2 - \theta_3) + c_2(\dot{\theta}_2 - \dot{\theta}_3) = 0 \quad (7)$$

$$I_3\ddot{\theta}_3 - k_2(\theta_2 - \theta_3) - c_2(\dot{\theta}_2 - \dot{\theta}_3) = 0 \quad (8)$$

This model is suitable to simulate the system configurations when the torque limiter in stick state.

Modal Analysis of the 3 dof model

A state-space representation is formulated in order to extract modal properties of the non-proportional viscous damping model according to Duncan's method:

$$\begin{bmatrix}[C] & [M]\\ [M] & [0]\end{bmatrix}_{6x6}\{\dot{y}\} + \begin{bmatrix}[K] & [0]\\ [0] & -[M]\end{bmatrix}_{6x6} = \{0\} \quad (9)$$

$$[A]\{\dot{y}\} + [B]\{y\} = \{0\} \quad (10)$$

where the state vector is defined as $\{y\} = \begin{Bmatrix}x\\ \dot{x}\end{Bmatrix}_{6x1}$. Equation (10) is a classic eigenvalue problem, whose solution consists of 6 complex eigenvalues λ_r and 6 complex eigenvectors $\{\vartheta\}_r$, that satisfy the following relationship:

$$(\lambda_r[A] + [B])\{\vartheta\}_r = \{0\} \quad (r = 1,2,\dots 6) \quad (11)$$

In what follows, the real solution of the eigenvalue problem associated with the undamped dynamic system is presented to simplify the discussion. Figure 29 shows the 3 real eigenvalues and the corresponding real eigenvectors of the undamped system. The left bar plot depicts the first mode which is the rigid body mode of the system; the central one shows the first flexible torsional mode of the powertrain, also known as shuffle or tip-in mode, in which the vehicle (inertia number 3) and the rest of the driveline (inertias number 1 and 2) are 180° out of phase. The third mode, visible in the right part of the figure, is the most relevant for this research: it is the torsional damper or DMF mode, where the primary and secondary flywheels have opposite phase. The DMF resonance frequency is very similar to the value computed with the detailed Amesim model.

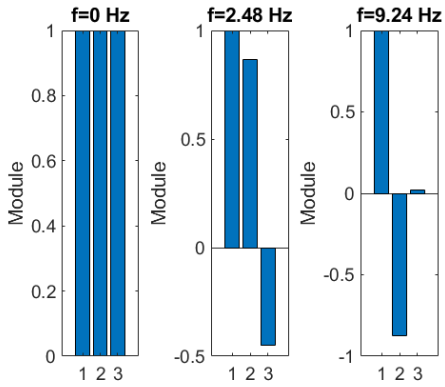

Figure 29. Eigenvectors and natural frequencies of the undamped system

Figure 30 plots the inertance frequency response functions (FRFs) for the three modelled inertias. The excitation is a harmonic torque, representing engine torque fluctuations, applied to the first dof, while the responses are evaluated as angular accelerations of each rotary inertia.

Since the focus of analysis is on DMF dynamic behavior when crossing its resonance, a simplified expression for the modal damping ratio in this condition is looked for. By analyzing the corresponding modal shape as reported in Figure 21 and 29, an equivalent single degree of freedom system can be identified, i.e. a two-mass dynamic system composed of the first and second inertia with the DMF torsional stiffness and damping in between.
The equivalent inertia of the two-mass system and the critical damping are:

$$I_{eq} = \frac{I_1 I_2}{I_1 + I_2} \tag{12}$$

$$c_{cr} = 2\sqrt{I_{eq}\, k_1} \tag{13}$$

Therefore, the equivalent damping coefficient of the DMF can be properly selected to achieve the desired damping factor for this specific mode:

$$c_1 = \xi\, c_{cr} \tag{14}$$

The curves are parameterized as a function of damping factor ξ; obviously, the higher its value, the lower the resonance peak at the DMF resonance frequency.

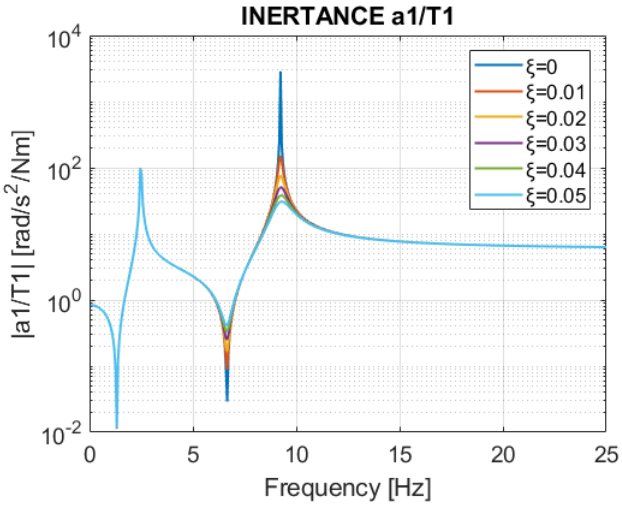

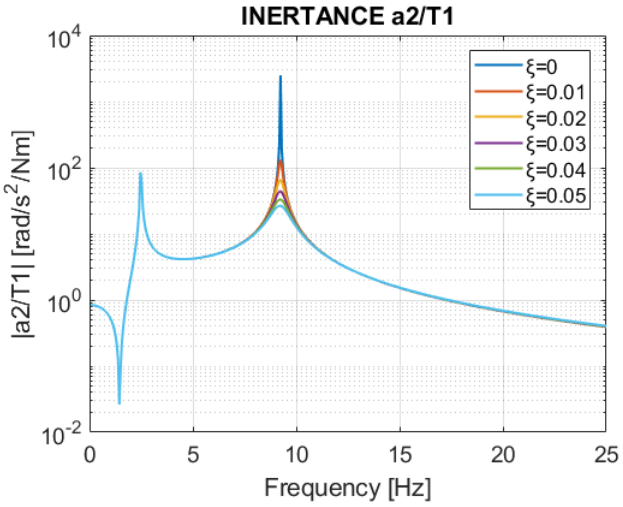

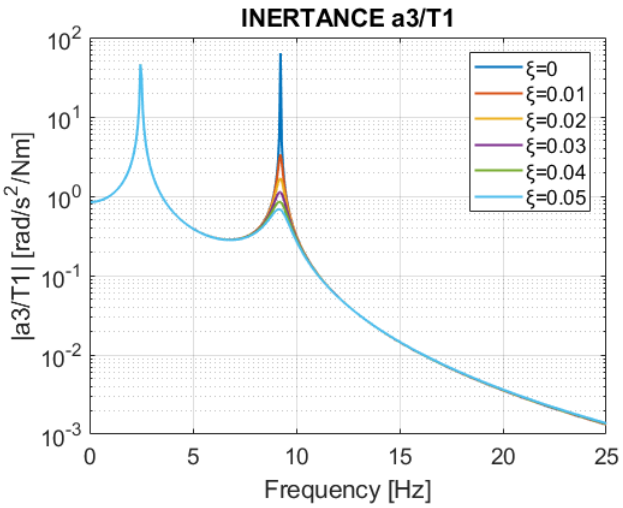

Figure 30. Frequency response functions: effect of DMF damping.

System nonlinearities and 4 dof model

The aim of the Simulink model is to represent also the nonlinear transient behavior of the torque limiter, due to its inherent characteristic of frictional coupling. The torque limiter is modelled as a friction clutch component that discriminates two different working conditions. The “stick phase” happens when the torque transferred by the torque limiter is lower than the slipping torque value and the difference between the velocities of drive plate and secondary flywheel

tends to zero; a 3 dof model is enabled in this case where drive plate and secondary inertia behave as a single solid unit.

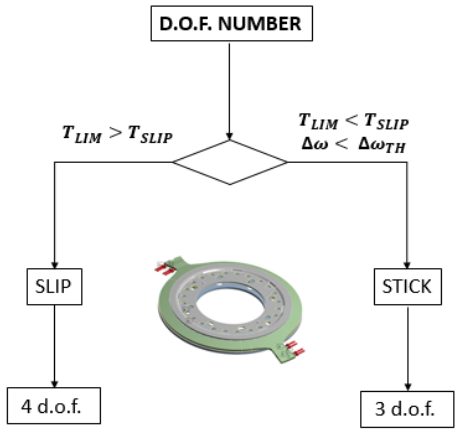

Figure 31. Flow chart for torque limiter state identification

The "slip phase" happens when the torque transmitted exceeds the slipping torque value or the relative speed is larger than zero; a 4 dof model is adopted because there is slippage between the drive plate and the secondary flywheel (Figure 31). The model is nonlinear non only because of dry friction between the limiter surfaces but also because of the arc spring characteristic elastic curve (see Figure 32).

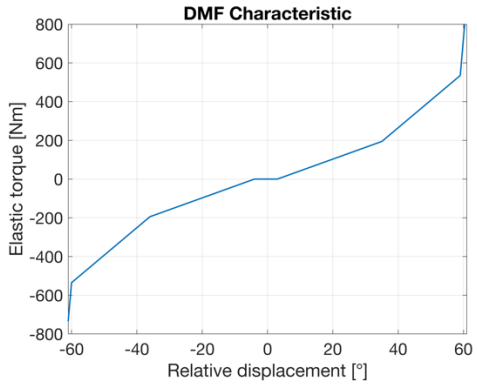

Figure 32. DMF elastic characteristic

As visible in Figure 32, the DMF shows a flat central zone where a certain amount of backlash is desirable for damping engine idle vibration, after that, the characteristic is piecewise linear. The first linear growing zone, with smaller slope, is designed for low to medium input torques and allows to keep resonance at low engine speeds. Then, the second zone, with a larger slope due to the presence of coaxial springs working in parallel, is dedicated for high engine torques.

As previously stated:

- if $|T_{LIM}| < T_{SLIP}$ and $|\Delta\omega| < \Delta\omega_{TH}$

a 3 dof model is used (Figure 33), described by the following equations

$$I_1\ddot{\theta}_1 + T_{DMF} + c_1(\dot{\theta}_1 - \dot{\theta}_2) = T_{in} \quad (15)$$

$$I_2^*\ddot{\theta}_2 - T_{DMF} - c_1(\dot{\theta}_1 - \dot{\theta}_2) + k_2(\theta_2 - \theta_3) + c_2(\dot{\theta}_2 - \dot{\theta}_3) = 0 \quad (16)$$

$$I_3\ddot{\theta}_3 - k_2(\theta_2 - \theta_3) - c_2(\dot{\theta}_2 - \dot{\theta}_3) = 0 \quad (17)$$

where I_2^* is the sum of drive plate and secondary flywheel moments of inertia and T_{DMF} is a nonlinear function of the DMF torsion angle, as reported in Figure 32;

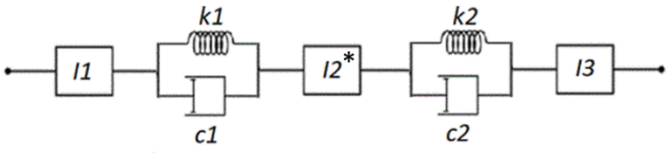

Figure 33. Three-d.o.f. model configuration

- if $|T_{LIM}| > T_{SLIP}$ or $|\Delta\omega| > \Delta\omega_{TH}$

the 4 dof case is enabled, it is modelled as:

$$I_1\ddot{\theta}_1 + T_{DMF} + c_1(\dot{\theta}_1 - \dot{\theta}_d) = T_{in} \quad (18)$$

$$I_d\ddot{\theta}_d - T_{DMF} - c_1(\dot{\theta}_1 - \dot{\theta}_d) + T_{LIM} = 0 \quad (19)$$

$$I_2\ddot{\theta}_2 - T_{LIM} + k_2(\theta_2 - \theta_3) + c_2(\dot{\theta}_2 - \dot{\theta}_3) = 0 \quad (20)$$

$$I_3\ddot{\theta}_3 - k_2(\theta_2 - \theta_3) - c_2(\dot{\theta}_2 - \dot{\theta}_3) = 0 \quad (21)$$

In this case, the drive plate I_d and the secondary flywheel I_2 are decoupled (Figure 34).

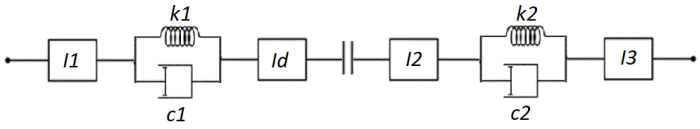

Figure 34. Four-dof. model configuration

The input torque T_{in} is the sum of the experimental engine and starter torques also used in the Amesim model.

Simulation results of the simplified model

In the most critical case, with 10% slope, Simulink model offers results similar to those obtained with Amesim. Without torque limiter, four overtorque peaks stress the DMF. Conversely, when the slipping device is used, the torque saturates, and the arc springs can work safely. The slipping torque is set to 1000 Nm; Figure 35 presents a higher value due to drive plate inertia and damping. Figure 36 shows that the torque limiter transmits the torque saturated at 1000 Nm.

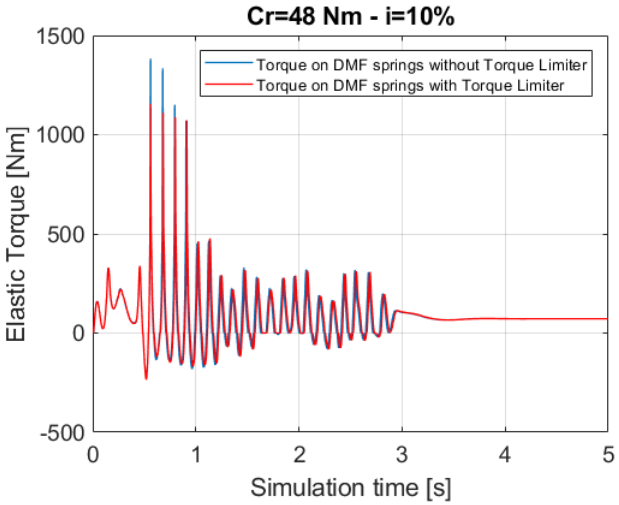

Figure 35. Elastic torque with and without torque limiter for 10% slope

An important parameter is the speed difference between drive plate and secondary flywheel; this speed difference identifies the slipping phases. Initially, there is no slippage between drive plate and secondary flywheel, so the relative speed is equal to zero. When torque becomes larger than the slipping value, the system shows two different velocities because torque limiter operates in slip mode (Figure 37). The slippage continues intermittently until stick condition is finally reached.

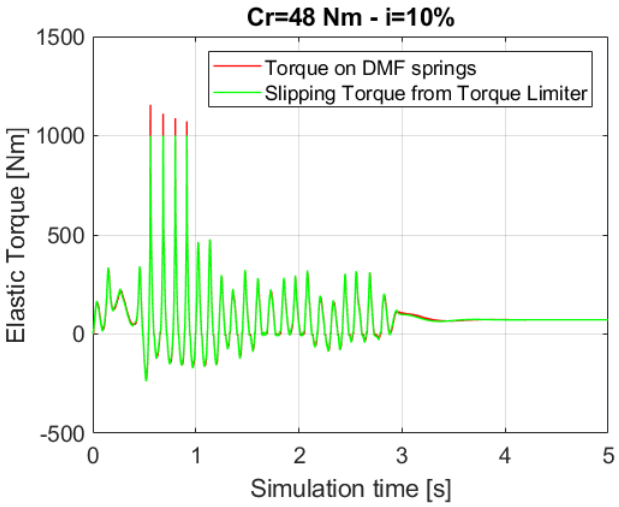

Figure 36. Torque transferred by torque limiter at 10% road slope.

Figure 37 shows drive plate and secondary flywheel velocities in the first part of the simulation where there are several transitions between stick and slip state in the torque limiter model. When the torque exceeds the slipping value, the drive plate firstly accelerates and then decelerates with respect to the secondary flywheel, thus allowing shock energy dissipation. As a consequence, the desired overtorques suppression function is achieved.

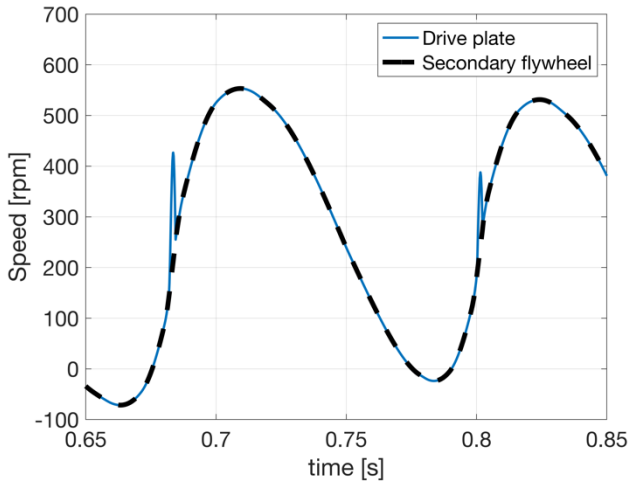

Figure 37. Particular of drive plate and secondary flywheel speed during the first two overtorque events.

Conclusions

This paper is focused on designing and modeling a torque limiter for its integration in a Dual Mass Flywheel, aimed at suppressing torsional shocks, called overtorques.

A technical solution for limiting overtorques in a DMF, based on the adoption of a tapered drive plate preloaded by two retainer plates, is discussed in detail. The paper also describes the experimental testing activity to verify torque limiter performance and reliability.

By adopting the torque limiter in combination with a DMF, the maximum torque transferred by the elastic elements is limited to its slipping torque value, thus avoiding structural damages to the arc spring and other transmission components. Since the effect of the torque limiter is a saturation of the maximum torque value transferred through it, its effect can be seen only in the presence of overtorques and not in the normal working condition of the DMF where the vibrational behavior of the system remains unchanged.

The dynamic transient behavior of DMF equipped with torque limiter has been described and analyzed both in time and frequency domain. Two different lumped-parameter models, a detailed Amesim model for quantitative analysis and a simplified Simulink model for torque limitation concept verification, have been proposed. The comparison of simulation results shows the efficacy of both models to predict the beneficial effect of the torque limiter in reducing torsional shocks and vibrations.

References

1. Galvagno, E., Tota, A., Velardocchia, M., and Vigliani, A., “Enhancing Transmission NVH Performance through Powertrain Control Integration with Active Braking System”, SAE Technical Papers, 2017, doi: 10.4271/2017-01-1778.
2. Amisano, F., Galvagno, E., Velardocchia, M., and Vigliani, A., “Automated manual transmission with a torque gap filler part 1: Kinematic analysis and dynamic analysis”, Proc. of Inst. Mechanical Engineers, Part D: Journal of Automobile Engineering, 2014, 228 (11): 1247-1261.

3. Galvagno, E., Velardocchia, M., Vigliani, A., “Torsional Oscillations in Automotive Transmissions: Experimental Analysis and Modelling”, Hindawi Publishing Corporation, Shock and Vibration 2016, 5:1-14, doi: 10.1155/2016/5721960.
4. L. Wei and W. K. Shi, “Summary of studies on dual mass flywheel (DMF)”, Noise and Vibration Control, 2008, 28: 1–5.
5. He, L.; Xia, C.; Chen, S.; Guo, J.; Liu, Y., “Parametric Investigation of Dual-Mass Flywheel Based on Driveline Start-Up Torsional Vibration Control”, Shock Vib., 2019:1-12, doi: 10.1155/2019/3171698.
6. Galvagno, E., Velardocchia, M., Vigliani, A., and Tota, A., “Experimental Analysis and Model Validation of a Dual Mass Flywheel for Passenger Cars”, SAE Technical Paper 2015-01-1121, 2015, doi:10.4271/2015-01-1121.
7. Schnurr, M., “Development of the Super-Long-Travel Dual Mass Flywheel”, LUK, 4th International Symposium, Baden-Baden, 1990.
8. Vitaliani, E., Di Rocco, D., and Sopouch, M., “Modelling and Simulation of General Path Centrifugal Pendulum Vibration Absorbers”, SAE Technical Paper 2015-24-2387, 2015, doi:10.4271/2015-24-2387.
9. Ragupathy, R., Pothiraj, K., Chendil, C., Kumar Prasad, T. et al., “Powertrain Torsional Impact Load Causes, Effects and Mitigation Measures in a Parallel Mild Hybrid Powertrain”, SAE Technical Paper 2016-01-1062, 2016, doi:10.4271/2016-01-1062.
10. Deutsches Institut für Normung. (2006). Disc Springs – Calculation DIN 2092:2006-03. Berlin, Germany.
11. Reik, W., Seebacher, R., Kooy A., “Dual Mass Flywheel”, 6th International Symposium, BadenBaden: LuK Buhl, 1998: 69-94.

Acknowledgments

The authors wish to thank Eng. Massimo Cima and Cristiano Baudino of Valeo for their valuable support in providing experimental data, simulation tools and for sharing their experience in transmission component design and testing.

Definitions/Abbreviations

dof	Degree of freedom
DMF	Dual Mass Flywheel
f	Frequency
I	Mass Moment of Inertia
k	Torsional stiffness
mdof	Multiple degrees of freedom
T	Torque
t	Time
ω	Angular speed
$\boldsymbol{\theta}, \dot{\boldsymbol{\theta}}, \ddot{\boldsymbol{\theta}}$	Angular position, velocity and acceleration